SOLID FREEFORM FABRICATION OF FUNCTIONAL SILICON NITRIDE CERAMICS BY LAMINATED OBJECT MANUFACTURING

S. J. Rodrigues, R.P. Chartoff, D.A. Klosterman, M. Agarwala, and N. Hecht

The University of Dayton

Rapid Prototype Development Laboratory

Dayton, Ohio 45469-0130

USA

ABSTRACT

The processing of silicon nitride (Si_3N_4) structural ceramics by Laminated Object Manufacturing (LOM) using ceramic tape preforms was investigated. The key processing stages involved green shape formation (which used the LOM process), followed by the burnout of all organics, and final densification by pressureless sintering. Two material systems were considered. These were a) monolithic Si_3N_4 and b) a preceramic polymer infiltrated Si_3N_4. The raw materials for the process were tape preforms of Si_3N_4, which were fabricated by standard tape casting techniques.

Mechanical property data obtained for the LOM processed Si_3N_4 showed high strength and fracture toughness values. The room temperature and high temperature (1260 ^oC) flexural strengths were in the range of 700-900 MPa and 360-400 MPa, respectively. The fracture toughness averaged from 5.5-7.5 $MPa.m^{1/2}$. These strength and fracture toughness values are comparable to those reported for conventionally prepared Si_3N_4 ceramics. Thus, this research demonstrated that the LOM technique is a viable method for preparing functional Si_3N_4 ceramics with good physical and mechanical properties.

INTRODUCTION

The LOM process is a Rapid Prototyping (RP) technique, which enables the Solid Freeform Fabrication (SFF) of a physical three-dimensional (3-D) part of arbitrary shape directly from a numerical CAD representation of the object. The process is based on the principle of sequentially laminating constituent cross-sections to fabricate the object.

The feasibility of using the LOM technique to fabricate advanced structural ceramics has been successfully demonstrated by a number of researchers [1-4]. The ceramics fabricated include high - density alumina (Al_2O_3) [1], monolithic zirconium oxide (ZrO_2) and composite ZrO_2 /Al_2O [2], SiC and SiC/SiC composites [3,4]. The properties of the LOM components were similar to the physical and mechanical properties of the ceramics prepared by conventional processes.

In this study a modified LOM machine (Model LOM-2030, Helisys, Inc., Torrance, CA) was used with green Si_3N_4 ceramic tapes to manufacture ceramic parts. The tapes were fabricated using Si_3N_4 powder along with polymeric additives and plasticizers. The LOM machine was used to sequentially laminate and cut (green tape) cross sections of the part being fabricated from the bottom to the top of the part. Excess material surrounding the green part was removed. The part, then, underwent a process of binder burnout to remove organics. The final step involved sintering to a higher density in a conventional furnace. An alternative process involved infiltration of a preceramic polymer into powder compacts formed by binder burnout. The use of high green density tape preforms as the starting material gives the LOM process an advantage over other SFF processes in obtaining high density final parts. In this report the physical and mechanical properties of the LOM Si_3N_4 are reported and the potential for manufacturing complex shaped components by the LOM process is demonstrated.

EXPERIMENTAL PROCEDURES

Two material systems were investigated in this study. These were; a) monolithic Si_3N_4 and b) a preceramic polymer infiltrated Si_3N_4. The test specimens fabricated were square plates. In addition some more complex parts were fabricated by the LOM process for the purpose of investigating shrinkages. The key processing steps in the preparation of LOM Si_3N_4 components include: a) Si_3N_4 tape fabrication, b) green shape forming using LOM, c) post LOM processing, and d) densification.

Silicon Nitride Tapes

The quality of the green tapes determines most of the properties of the final product. Thus, green Si_3N_4 tapes with a high degree of homogeneity and uniform thickness were fabricated using standard tape casting technique [5], tailored for the LOM process. A high purity, submicron (average particle size = 0.7 μm), alpha phase silicon nitride (α-Si_3N_4) powder along with Yttria (Y_2O_3), and alumina (Al_2O_3) as sintering aids were used in this study to prepare the Si_3N_4 tapes. These tapes were formulated with an acrylic binder system and a plasticizer to provide for the required flexibility and appropriate adhesion during the LOM layup process.

Producing Greenforms Using LOM

Producing the desired shapes for the green compacts was done using the standard LOM stack-then-cut approach. Two key unit operations in the process are laser cutting and lamination. The geometry of the cross-sectional area corresponding to each layer is defined by the laser cutting. The laser also dices or cubes the excess material, which is eventually removed. Lamination serves two important roles in the process. First, it provides good “tacking” and second, complete fusion between individual green layers. Good “tacking” helps preserve registration during stacking, which is required for the preservation of the geometry of the part being built. Effective lamination is necessary to fuse the tape stack into a seamless monolith to obtain a homogeneous compact. In this study thermal lamination, without solvent assist, was utilized to obtain good tacking and fusion of individual layers. The key machine parameters included the laser power, cutting speed, roller temperature, and roller speed. These must be optimized to achieve the required results.

Post LOM Processing

The post LOM processing involved binder burnout and, in some cases, a preceramic polymer infiltration. The polymeric components in the Si_3N_4 greenforms were expelled by pyrolysis in two stages. The first stage involved heating the samples embedded in fine Al_2O_3 powder, with flowing N_2 gas to 500 ^oC. The second stage involved further heating of the samples in air to 500 ^oC to eliminate the residual carbonaceous material.

In one set of experiments a preceramic polymer was infiltrated into the porous preforms after binder burnout. Ceraset^{TM}SN (Commodore Polymer Technologies Inc., New York, NY, U.S.A.), a solvent free, liquid preceramic polymer, was selected as the infiltrant. Ceraset is a thermosetting, polyurea-silazane based resin, with alternate silicon (Si) and nitrogen (N) atoms that form the chain backbone and vinyl appendages for facilitating a crosslinking reaction [6]. In the uncured state Ceraset is a low viscosity liquid. Infiltration was carried out by completely immersing samples in Ceraset. Subsequently, the infiltrated specimens were heated to 200 ^oC to cure the polymer and further pyrolyzed in flowing argon (Ar) atmosphere at 1000 ^oC.

Densification

Densification of the LOM Si_3N_4 compacts, both uninfiltrated and infiltrated was achieved by placing samples in a loosely packed protective bed of 30 wt.% BN-Si_3N_4 powder mixture to provide a local SiO partial pressure to minimize Si_3N_4 decomposition. The samples were fired in a sintering furnace at 1750 ^oC at a heatup rate of 5 ^oC/min with a 2 h final soak, under an N_2 atmosphere.

Composition and Microstructure Characterization

X-ray diffraction (XRD) was utilized to identify primary and secondary crystalline phases present in the bulk ceramics. Characterization of the morphology and microstructure was accomplished by Scanning Electron Microscopy (SEM).

Physical Properties

Bulk density measurements of sintered specimens were obtained using the ASTM C 373 procedure based on Archemedes principle. The weight loss and shrinkage measurements were determined from the physical dimensions of the sintered specimens.

Mechanical Properties

The ASTM C 1259 procedure was used for the determination of the dynamic Young's Modulus based on the resonant frequency of the specimens in the flexural vibration mode. Four-point flexural strengths of LOM Si_3N_4 were determined at room temperature and at 1260 ^oC using ASTM 1161-90 and ASTM 1211-92, respectively. Test bars 3 mm x 4 mm x 25.4 mm were cut and machined from the sintered specimens. A diamond wafering saw was used to cut test bars and the surfaces of the test bars were ground using a diamond grinding wheel (320 grit). Both room temperature and elevated temperature flexural tests were conducted in air with a crosshead speed of 5 mm/min.

In this project fracture toughness was measured using the Single Edge V-Notch Beam (SEVNB) method [8]. Rectangular test bars (L = 25 mm, W = 3.375 mm, T = 2.56 mm) were cut and machined using a 320-grit diamond-grinding wheel from sintered specimens. A diamond saw blade was then utilized to cut a notch in the samples. Subsequently, a razor blade was placed in the starter notch filled with diamond paste to create a V-notch that extended beyond the starter notch. The V-notch was placed on the tensile side of the test specimen and a crosshead speed of 5 mm/min was used. The peak load at fracture was determined and the depth of the V-notch was measured. Based on this information the fracture toughness K_{IC} was calculated. The ASTM E 384-89 procedure was used to calculate the Vickers hardness number for microhardness by forming indentations with a certain applied load on polished bars.

RESULTS AND DISCUSSION

Flexible Si_3N_4 green tapes with an average thickness of 0.19 mm (7.5 mils) and average green density of 56 % were fabricated. The tapes were pliable with good structural integrity thus, making them easy to handle. Examination of the cross-sections of the green tapes indicated uniform powder and pore distribution.

The optimized laser power and cutting speed aided in obtaining a clean cut kerf region as shown in Fig. 1. The cut-region profile is controlled by the Gaussian intensity profile of the laser beam; thus the kerf region is tapered. Lamination quality during the shape-forming process is evident from the photomicrograph (Fig. 2a) showing a cross-section of a 24 layer green Si_3N_4 specimen. The structure is homogeneous without any lamination lines. Fusion of layers was maintained during binder burnout. The burnout powder compact also is a seamless monolith (Fig. 2b).

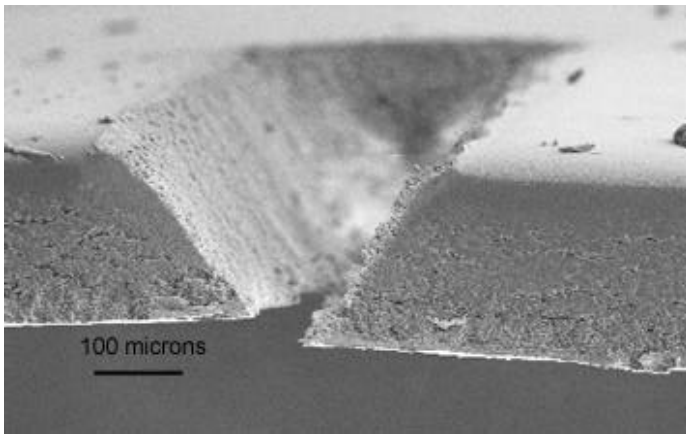

Fig. 1 Si_3N_4 tape laser-cut region with cutting speed and laser power of 6.35 cm/s and 8 W, respectively.

Densification was accomplished by a liquid phase sintering process, whereby α-Si_3N_4 melts in a eutectic liquid formed by the reaction between the sintering aids and the oxide layer on the surface of Si_3N_4 and reprecipitates as β-Si_3N_4. The microstructure of a sintered monolithic

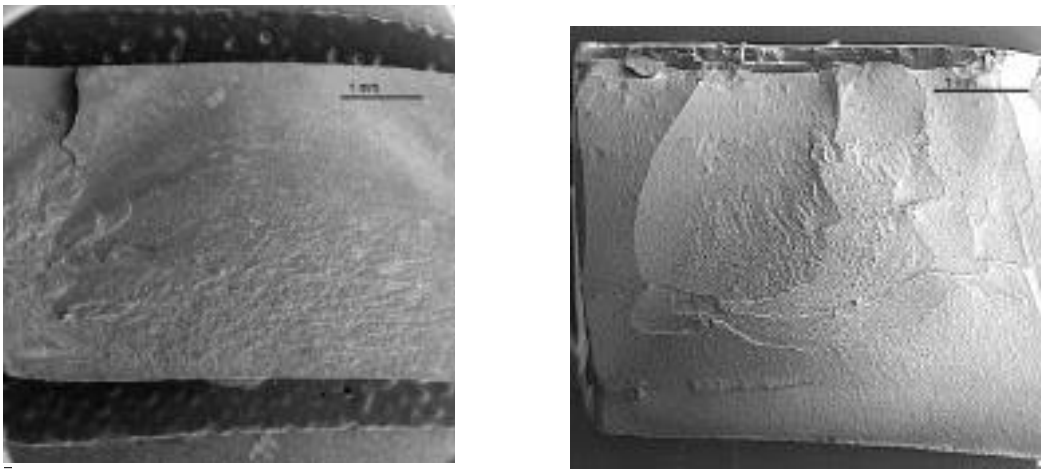

(a) (b)

Fig. 2 Cross-section of a 24-layer S_3N_4 a) green and b) binder burnout specimen.

Si_3N_4 without any infiltrated preceramic polymer is shown in Fig. 3. Elongated β-Si_3N_4 grains are observed having an aspect ratio of 6, with an average long and short axis dimension of 1.2 μm and 0.2 μm, respectively. A small retention of α-Si_3N_4 is evident from XRD data. The α/β ratio is approximately 0.1 for the (101) plane.

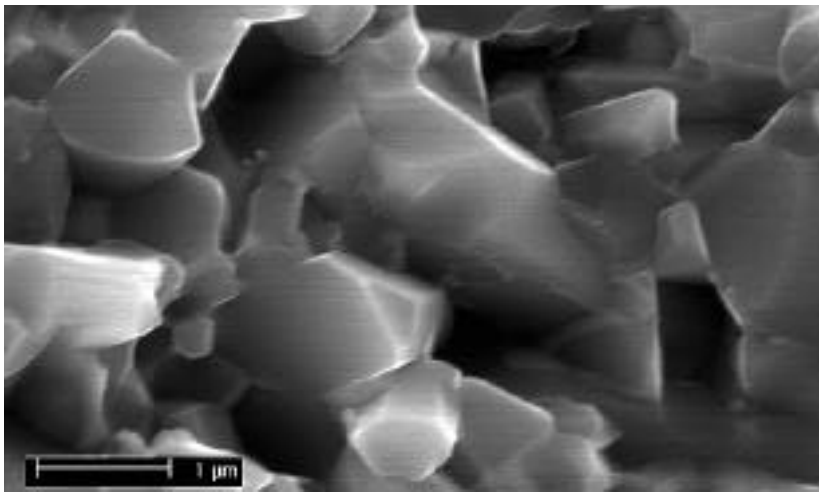

Fig. 3 Fracture surface of densified LOM Si_3N_4 specimen without any infiltration.

The microstructure of the sintered LOM Si_3N_4 system infiltrated with the preceramic polymer, presented in Fig. 4, shows both re-precipitated, elongated β-Si_3N_4 grains and fine equiaxed α-Si_3N_4 grains. The aspect ratio of β-Si_3N_4 in this case was approximately 4.5. In this case XRD analysis of samples showed the retention of a large amount of α-Si_3N_4 phase. This is apparent from the peak intensities of the (101) plane. The α/β ratio (0.4) is higher than in the case without polymer infiltration.

The physical properties of both uninfiltrated and infiltrated specimens are tabulated in Table 1 and compared to property values for conventionally prepared Si_3N_4. Theoretical density

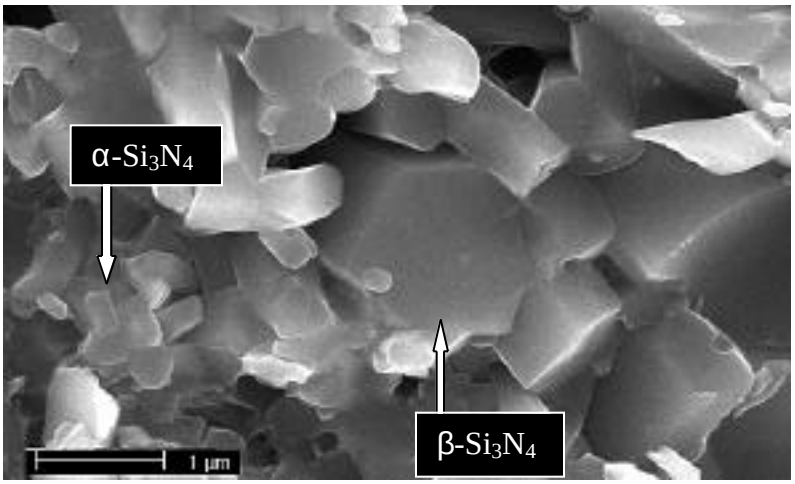

Fig. 4 Fracture surface of densified LOM Si_3N_4 specimen infiltrated with preceramic polymer Ceraset.

was calculated using a linear relation from the densities of Si_3N_4 (3.18 g/cm^3), Al_2O_3 (3.98 g/cm^3) and Y_2O_3 (4.84 g/cm^3) and volume percent of each component present in the system. For the infiltrated specimens this also included the pyrolyzed Ceraset. It is assumed that all Ceraset was converted to Si_3N_4 on pyrolysis and sintering. The percent theoretical densities measured for the infiltrated specimens were less than those measured for the uninfiltrated LOM Si_3N_4. This is attributed to the higher porosity in the infiltrated specimens, due to the outgassing of residual volatiles in the system. The inherent shrinkage that occurs on sintering is reduced in the case of the infiltrated specimens primarily due to the volume filling by the ceramic created by pyrolysis. The strong covalent bonding in Si_3N_4 results in a high modulus value, which is an average of the elastic moduli for the various crystallographic directions since the Si_3N_4 fabricated is polycrystalline.

The LOM Si_3N_4 specimens were found to have mechanical property values comparable to the ones made by conventional processes [8-10]. Data for both uninfiltrated and infiltrated LOM Si_3N_4 are presented in Table 2 along with the property values of conventionally prepared Si_3N_4. Each mechanical property value (average) was obtained using 5 test bars for both uninfiltrated and infiltrated LOM Si_3N_4.

Table 1: Physical Properties of LOM Si_3N_4 and conventional Si_3N_4.

	Avg. Density (g/cm^3)	Theoretical Density (%)	Avg.Volume shrinkage (%)
Uninfiltrated LOM Si_3N_4	3.248	97	40
Infiltrated LOM Si_3N_4	3.142	94	25
Conventional Si_3N_4*	2.2-3.9	70-100	-

* property values are dependent on type of processing used in fabrication [8-10].

Table 2: Mechanical Properties of LOM Si_3N_4 and conventional Si_3N_4.

	Avg. Young's Modulus (GPa)	Avg. R. T.* Flexural Strength (MPa)	Avg. H.T.* Flexural Strength (MPa)	Avg. Fracture Toughness ($MPa.m^{1/2}$)	Avg. Vickers Microhardness (Kgf/mm^2)
Uninfiltrated LOM Si_3N_4	307	918	400	7.45	1457
Infiltrated LOM Si_3N_4	301	707	361	5.42	1379
Conventional Si_3N_4**	100-320	200-1200	180-800	1.5-8.2	1000-2000

* R.T. = Room Temperature, H.T. = High Temperature ($1260\ ^0C$)

**property values are dependent on type of processing used in fabrication [8-10].

The higher room temperature flexural strength values for the case of uninfiltrated specimens compared to infiltrated specimens are due to higher densities. The inherent increase in flaw population, caused by the additional step of infiltration during processing, also contributes to the decrease in strength for the infiltrated specimens. All test bars revealed linear elastic behavior from the onset of loading to brittle failure, prior to any perceivable plastic deformation for both room and high temperatures, except for the infiltrated test bars at high temperature. In this case the deviation from linearity could be attributed to the occurrence of creep caused by grain boundary sliding. The reduction of strength at high temperature was 56 % and 48 % for the uninfiltrated and infiltrated specimens, respectively. The amorphous phase resulting from the oxide sintering aids softens at high temperature causing the reduction of strength. The fracture modes in all test bars included both intergranular and transgranular fractures. The increased fracture toughness values obtained for the uninfiltrated specimens are a reflection of the higher aspect ratio and percent β-Si_3N_4 present in the system compared to the infiltrated test bars. The high Vickers microhardness number for all test bars are a measure of the materials resistance to localized plastic deformation and are comparable to conventionally prepared Si_3N_4.

Complex-shape Components

The potential to form complex shapes without molds or dies is an asset of the LOM process. A model complex-shape Si_3N_4 gear component was fabricated to demonstrate the capability of the LOM process. Both infiltrated and uninfiltrated gears were fabricated. Fig. 5 shows 25 layer green and sintered forms. The inherent shrinkage is reduced in the case of the infiltrated component. The volume percent shrinkage is reproducible and needs to be taken into account when designing complex-shapes.

CONCLUSIONS

The SFF of advanced Si_3N_4 structural components based on the LOM process has been investigated and was demonstrated to be a viable process. Green Si_3N_4 ceramic tapes with high

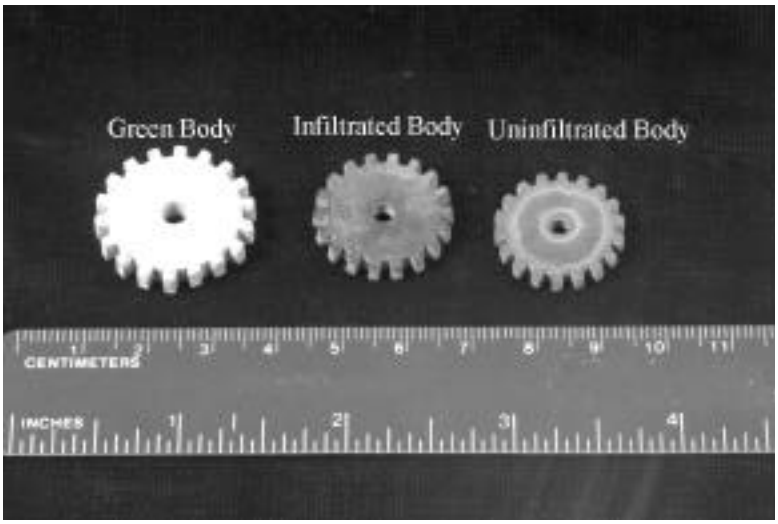

Fig. 5 Complex-shaped Si_3N_4 components formed by the LOM process.

ceramic loading and properties tailored for the LOM process were fabricated and used to prepare Si_3N_4 components. These were consolidated to high densities by pressureless sintering. In this study the processing stages involved in the powder-to-part fabrication of advanced Si_3N_4 ceramic parts were optimized and material characteristics of the final parts were evaluated. The material characteristics evaluated included the microstructures, as well as physical, and mechanical properties. The resulting physical and mechanical properties of the sintered LOM Si_3N_4 were competitive with Si_3N_4 prepared by conventional methods such as reaction-bonding, conventional shape-forming (e.g. slip casting), and pressureless sintering. The potential for fabricating complex-shape components from LOM greenforms also was demonstrated.

REFERENCES

1. C. Griffin, J. Daufenbach, and S. McMillin, *Solid Freeform Fabrication Symposium Proceedings*, University of Texas, Austin, TX, pp. 17, (1994).
2. E. A. Griffin, D. R. Mumm, and D. B. Marshall, *American Ceramic Society Bulletin*, **75**, [7], 65 (1996).
3. D. Klosterman, R. Chartoff, N. Osborne, G. Graves, A. Lightman, G. Han, A. Bezeredi, S. Rodrigues, *American Ceramic Society Bulletin*, **77**, [10], 69, (1998).
4. D. Klosterman, R. Chartoff, N. Osborne, G. Graves, A. Lightman, G. Han, A. Bezeredi, and S. Rodrigues, *Rapid Prototyping Journal*, **5,** [2], 61, (1999).
5. R. Mistler, *Ceramic Bulletin*, **69**, 1022, (1990).
6. J.M. Schwark, and M.J. Sullivan, MRS Symposium Proceeding, **271**, 807, (1992).
7. J. Kubler, VAMAS TWP 31 ESIS T6, Swiss Federal Laboratories for Material Testing and Research, Switzerland (1997).
8. M. L. Torti, Structural Ceramics: Treatise on Materials Science and Technology, vol. 29, Academic Press Inc., New York, (1989).
9. J. R. Smyth, Ceramics and Glasses, vol. 4, Engineered Materials Handbook, American Society of Materials International, (1991).
10. U. T. Taffner, V. Carle, U. Schafer et at., *Pract., Met.,* **28,** 592, (1991)